

Velocity continuation by spectral methods

*Sergey Fomel*¹

ABSTRACT

I apply Fourier and Chebyshev spectral methods to derive accurate and efficient algorithms for velocity continuation. As expected, the accuracy of the spectral methods is noticeably superior to that of the finite-difference approach. Both methods apply a transformation of the time axis to squared time. The Chebyshev method is slightly less efficient than the Fourier method, but has less problems with the time transformation and also handles accurately the non-periodic boundary conditions.

INTRODUCTION

In a recent work (Fomel, 1994, 1996), I introduced the process of *velocity continuation* to describe a continuous transformation of seismic time-migrated images with a change of the migration velocity. Velocity continuation generalizes the ideas of residual migration (Rothman et al., 1985; Etgen, 1990) and cascaded migrations (Larner and Beasley, 1987). In the zero-offset (post-stack) case, the velocity continuation process is governed by a partial differential equation in midpoint, time, and velocity coordinates, first discovered by Claerbout (1986b). Hubral et al. (1996) and Schleicher et al. (1997) describe this process in a broader context of “image waves”. Generalizations are possible for the non-zero offset (prestack) case (Fomel, 1996, 1997).

A numerical implementation of velocity continuation process provides an efficient method of scanning the velocity dimension in the search of an optimally focused image. The first implementations (Li, 1986; Fomel, 1996) used an analogy with Claerbout’s 15-degree depth extrapolation equation to construct a finite-difference scheme with an implicit unconditionally stable advancement in velocity. Fomel and Claerbout (1997) presented an efficient three-dimensional generalization, applying the helix transform (Claerbout, 1997).

A low-order finite-difference method is probably the most efficient numerical approach to this method, requiring the least work per velocity step. However, its accuracy is not optimal because of the well-known numerical dispersion effect. Figure 1 shows impulse responses of post-stack velocity continuation for three impulses, computed by the second-order finite-difference method (Fomel, 1996). As expected from the residual migration theory (Rothman et al., 1985), continuation to a higher velocity (left plot) corresponds to migration with a residual velocity, and its impulse responses have an elliptical shape. Continuation to a smaller velocity

¹email: sergey@sep.stanford.edu

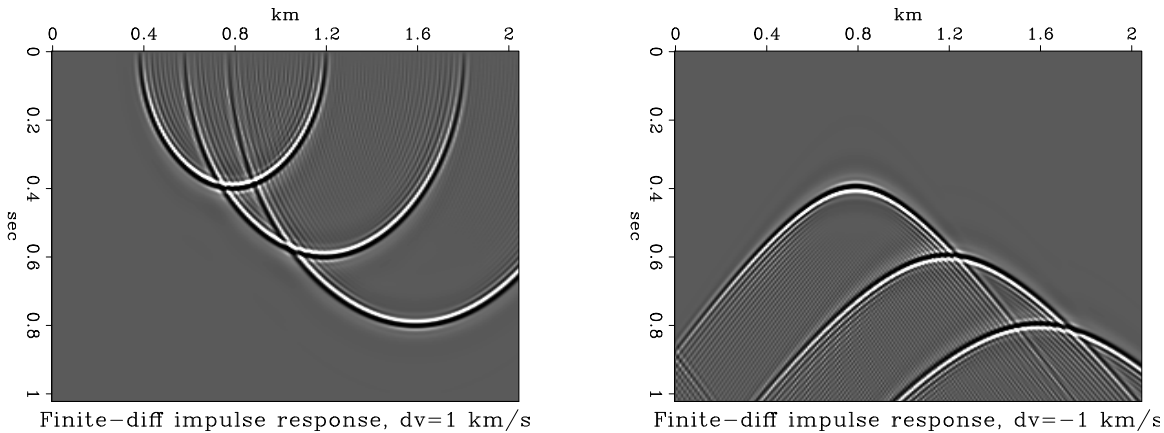


Figure 1: Impulse responses (Green's functions) of velocity continuation, computed by a second-order finite-difference method. The left plots corresponds to continuation to a larger velocity (+1 km/sec); the right plot, smaller velocity, (-1 km/sec). `velspec-fd-imp` [ER]

(right plot in Figure 1) corresponds to demigration (modeling), and its impulse responses have a hyperbolic shape. The dispersion artifacts are clearly visible in the figure.

In this paper, I explore the possibility of implementing a numerical velocity continuation by spectral methods. I adopted two different methods, comparable in efficiency with finite differences. The first method is a direct application of the Fast Fourier Transform (FFT) technique. The second method transforms the time grid to Chebyshev collocation points, which leads to an application of the Chebyshev- τ method (Lanczos, 1956; Gottlieb and Orszag, 1977; Boyd, 1989), combined with an unconditionally stable implicit advancement in velocity. Both methods employ a transformation of the grid from time t to the squared time $\sigma = t^2$, which removes the dependence on t from the coefficients of the velocity continuation equation. Additionally, the Fourier transform in the space (midpoint) variable x takes care of the spatial dependencies. This transform is a major source of efficiency, because different wavenumber slices can be processed independently on a parallel computer before transforming them back to the physical space.

PROBLEM FORMULATION

The post-stack velocity continuation process is governed by a partial differential equation in the domain, composed by the seismic image coordinates (midpoint x and vertical time t) and the additional velocity coordinate v . Neglecting some amplitude-correcting terms (Fomel, 1996), the equation takes the form (Claerbout, 1986b)

$$\frac{\partial^2 P}{\partial v \partial t} + vt \frac{\partial^2 P}{\partial x^2} = 0. \quad (1)$$

Equation (1) is linear and belongs to the hyperbolic type. It describes a wave-type process with the velocity v acting as a “time-like” variable. Each constant- v slice of the function $P(x, t, v)$

corresponds to an image with the corresponding constant velocity. The necessary boundary and initial conditions are

$$P|_{t=T} = 0 \quad P|_{v=v_0} = P_0(x, t), \quad (2)$$

where v_0 is the starting velocity, $T = 0$ for continuation to a smaller velocity and T is the largest time on the image (completely attenuated reflection energy) for continuation to a larger velocity. The first case corresponds to “modeling”; the latter case, to seismic migration.

Mathematically, equations (1) and (2) define a Goursat-type problem (Courant, 1962). Its analytical solution can be constructed by a variation of the Riemann method in the form of an integral operator (Fomel, 1994, 1996):

$$P(t, x, v) = \frac{1}{(2\pi)^{m/2}} \int \frac{1}{(\sqrt{v^2 - v_0^2} \rho)^{m/2}} \left(-\frac{\partial}{\partial t_0} \right)^{m/2} P_0 \left(\frac{\rho}{\sqrt{v^2 - v_0^2}}, x_0 \right) dx_0, \quad (3)$$

where $\rho = \sqrt{(v^2 - v_0^2)t^2 + (x - x_0)^2}$, $m = 1$ in the 2-D case, and $m = 2$ in the 3-D case. In the case of continuation from zero velocity $v_0 = 0$, operator (3) is equivalent (up to the amplitude weighting) to conventional Kirchoff time migration (Schneider, 1978). Similarly, in the frequency-wavenumber domain, velocity continuation takes the form

$$\hat{P}(\omega, k, v) = \hat{P}_0(\sqrt{\omega^2 + k^2(v^2 - v_0^2)}, k), \quad (4)$$

which is equivalent (up to scaling coefficients) to Stolt migration (Stolt, 1985), regarded as the most efficient migration method.

If our task is to create many constant-velocity slices, there are other ways to construct the solution of problem (1-2). Two alternative spectral approaches are discussed in the next two sections.

FOURIER APPROACH

Introducing the change of variable $\sigma = t^2$, we can transform equation (1) to the form

$$2 \frac{\partial^2 P}{\partial v \partial \sigma} + v \frac{\partial^2 P}{\partial x^2} = 0, \quad (5)$$

whose coefficients don't depend on the time variables. Double Fourier transform in σ and x further simplifies equation (5) to the ordinary differential equation

$$2i\Omega \frac{d^2 \hat{P}}{dv} - vk^2 \hat{P} = 0, \quad (6)$$

where the frequency Ω corresponds to the time coordinate σ , and k is the wavenumber in x . Equation (6) has an explicit analytical solution

$$\hat{P}(k, \Omega, v) = \hat{P}_0(k, \Omega) e^{\frac{ik^2(v_0^2 - v^2)}{4\Omega}}, \quad (7)$$

which defines a very simple algorithm for the numerical velocity continuation. The algorithm consists of the following steps:

1. Transform the input from a regular grid in t to a regular grid in σ .
2. Apply FFT in x and σ .
3. Multiply by the all-pass phase-shift filter $e^{\frac{ik^2(v_0^2 - v^2)}{4\Omega}}$.
4. Inverse FFT in x and σ .
5. Inverse transform to a regular grid in t .

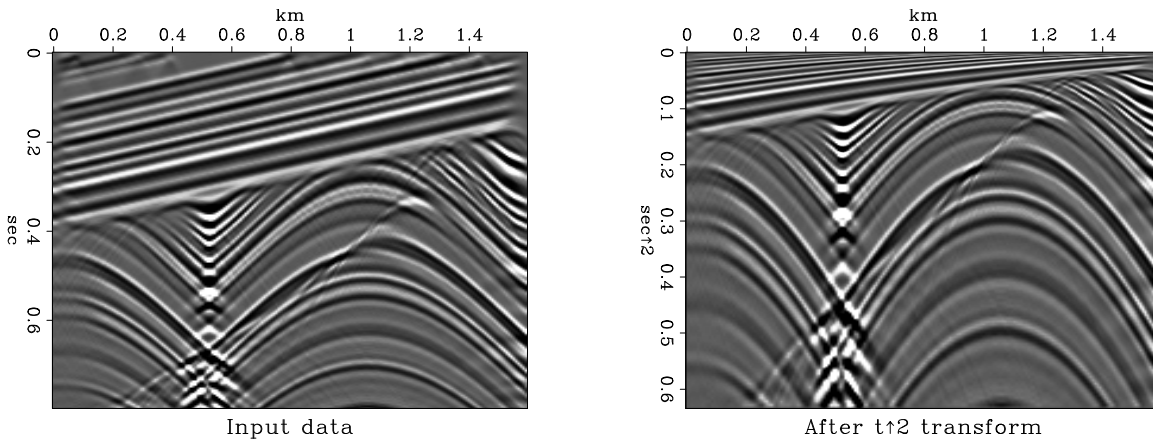


Figure 2: Synthetic seismic data before (left) and after (right) transformation to the σ grid. `velspec-t2` [ER]

Figure 2 shows a simple synthetic model of seismic reflection data from (Claerbout, 1995) before and after transforming the grid, regularly spaced in t , to a grid, regular in σ . The left plot of Figure 3 shows the Fourier transform of the data. Except for the nearly vertical event, which corresponds to a stack of parallel layers in the shallow part of the data, the data frequency range is contained near the origin in the $\Omega - k$ space. The right plot of Figure 3 shows the phase-shift filter for continuation from zero imaging velocity (which corresponds to unprocessed data) to the velocity of 1 km/sec. The rapidly oscillating part (small frequencies and large wavenumbers) is exactly in the place, where the data spectrum is zero and corresponds to physically impossible reflection events. Algorithm (7) is very attractive from the practical point of view because of its efficiency (based on the FFT algorithm). The operations count is roughly the same as in Stolt migration (4): two forward and inverse FFTs and forward and inverse grid transform with interpolation (one complex-number transform in the case of Stolt migration). Algorithm (7) can be even more efficient than Stolt method because of the simpler structure of the innermost loop. However, its practical implementation faces two difficult problems: artifacts of the t^2 grid transform and wraparound artifacts

Improving the accuracy of the t^2 grid transform

The first problem is the loss of information in the transform to the t^2 grid. As illustrated in Figure 2, the shallow part of the data gets severely compressed in the t^2 grid. The amount

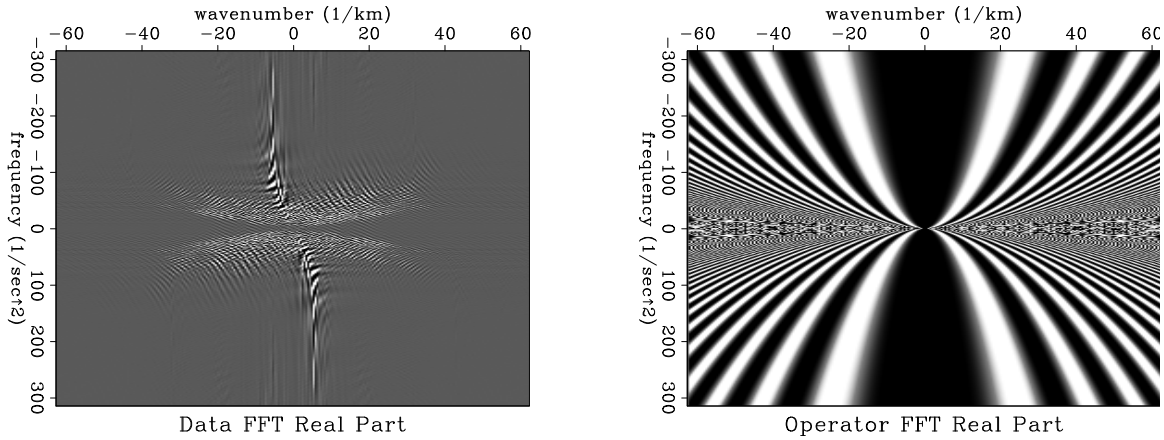


Figure 3: Left: the real part of the data Fourier transform. Right: the real part of the velocity continuation operator (continuation from 0 to 1 km/s) in the Fourier domain. `velspec-t2-fft` [ER]

of compression can lead to inadequate sampling, and as a result, aliasing artifacts in the frequency domain. Moreover, it can be difficult to recover from the loss of information in the transformed domain when transforming back into the original grid. A partial remedy for this problem is to increase the grid size in the t^2 domain. The top plots in Figure 4 show the result of back transformation to the t grid and the difference between this result and the original model (plotted on the same scale). We can see a noticeable loss of information in the upper (shallow) part of the data, caused by undersampling. The bottom plots in Figure 4 correspond to increasing the grid size by a factor of three. Some of the artifacts have been suppressed, at the expense of dealing with a larger grid. To perform an accurate transform of the grid, I adopted the following method, inspired by (Claerbout, 1986a). Let d_{new} denote the data on the new grid and d_{old} be the data on the old grid. If L is the interpolation operator, defined on the new grid, then the optimal least-square transformation is

$$d_{\text{new}} = (L^T L)^{-1} L d_{\text{old}}, \quad (8)$$

where L^T denotes the adjoint interpolation operator. The operator $(L^T L)^{-1}$ provides a proper scaling of the result. If we use simple linear interpolation for the L operator, then $L^T L$ is a tridiagonal matrix, which can be easily inverted (in $8N$ operations). If some parts in d_{new} are not fully constrained, then the tridiagonal matrix is not invertible. To obtain a solution in this case, we can include a regularization operator D in (8), as follows:

$$d_{\text{new}} = (L^T L + \epsilon^2 D)^{-1} L d_{\text{old}}, \quad (9)$$

A convenient choice for D is a second derivative operator, represented with the second-order finite-difference approximation. This operator allows the selection of the smoothest possible function d_{new} while preserving the efficient tridiagonal structure of $L^T L + \epsilon^2 D$. In this problem, the parameter ϵ can be chosen as small as possible, as long as it prevents the inversion from getting unstable.

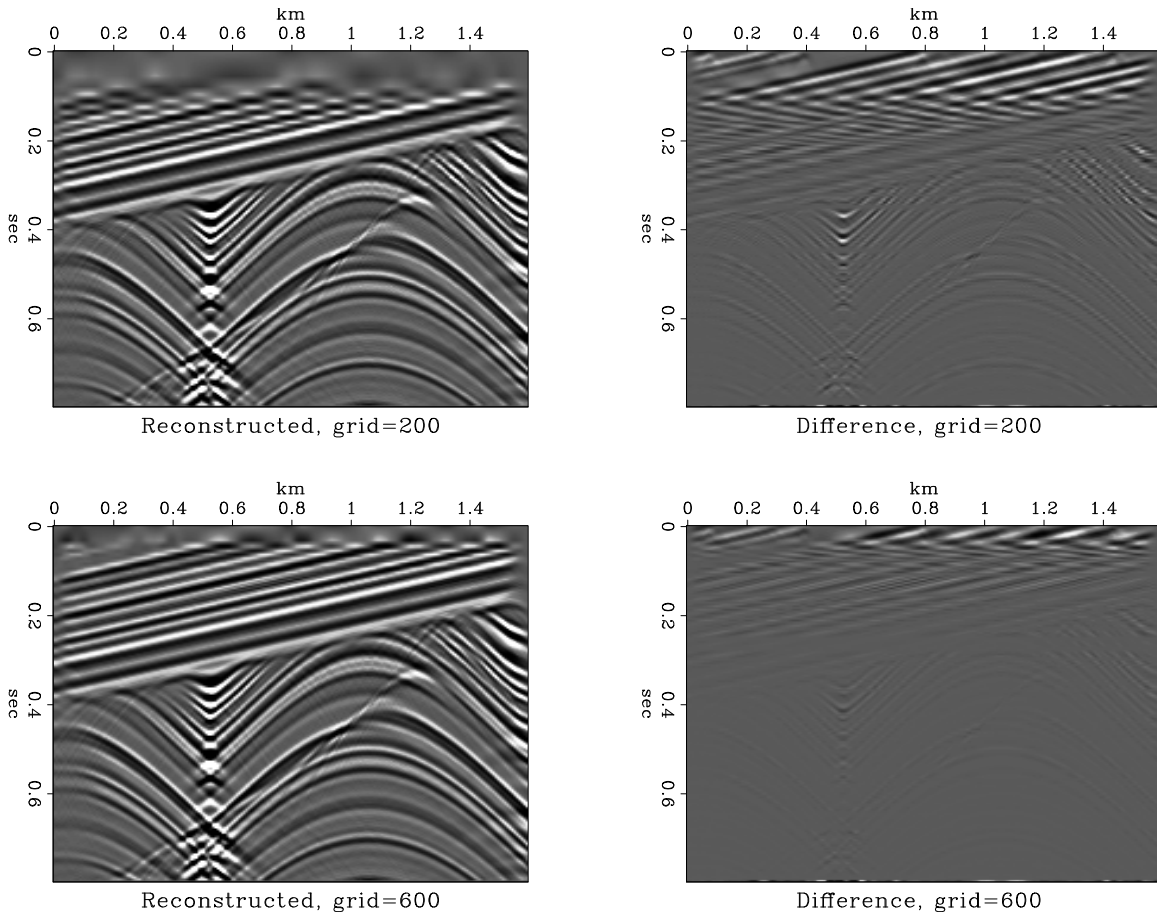


Figure 4: The left plots show the reconstruction of the original data after transforming back from the t^2 grid to the original t grid. The right plots show the difference with the original model. Top: using the original grid size ($N_t = 200$). Bottom: increasing the grid size by a factor of three. `velspec-fft-inv` [ER]

Suppressing wraparound artifacts of the Fourier method

The periodic boundary conditions both in the squared time σ and the spatial coordinate x , implied by the Fourier approach, are artificial in the problem of velocity continuation. The artificial periodicity is convenient from the computational point of view. However, false periodic events (wraparound artifacts) should be suppressed in the final output. A natural method for attacking this problem is to apply zero padding in the physical space prior to Fourier transform. Of course, this method involves an additional expense of the grid size increase.

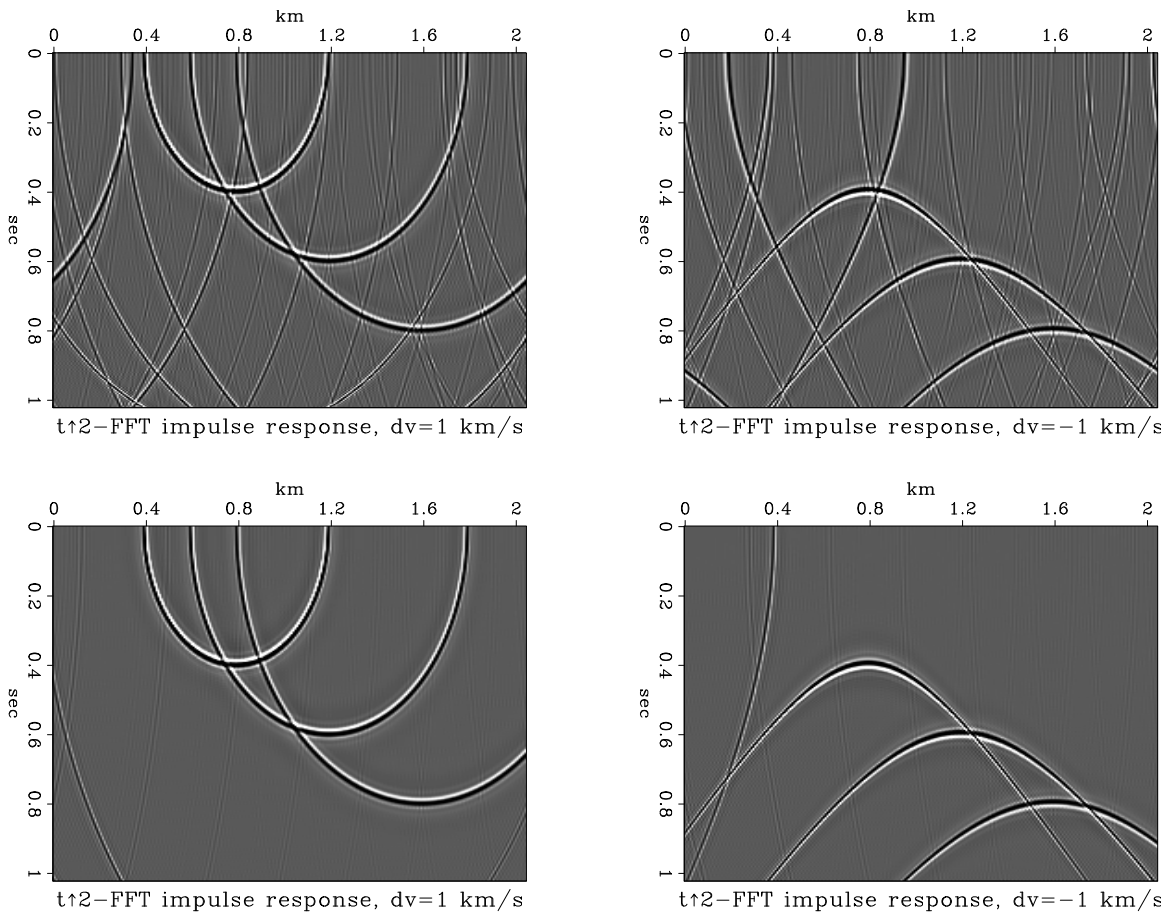


Figure 5: Impulse responses (Green's functions) of velocity continuation, computed by the Fourier method. Top: without zero padding, bottom: with zero padding. The left plots correspond to continuation to a larger velocity (+1 km/sec); the right plots, smaller velocity, (-1 km/sec). `velspec-fft-imp` [ER]

The top plots in Figure 5 show the numerical impulse responses of velocity continuation, computed by the Fourier method. The initial data contained three spikes, passed through a narrow-band filter. Theoretically, continuation to larger velocity (the left plot) should create three elliptical wavefronts, and continuation to smaller velocity (right plot) should create three hyperbolic wavefronts (Rothman et al., 1985). We can see that the results are largely contaminated with wraparound artifacts. The result of applying zero padding (the bottom plots in Figure 5) shows most of the artifacts suppressed.

Chebyshev spectral method, discussed in the next section, provides a spectral accuracy while dealing correctly with non-periodic data.

CHEBYSHEV APPROACH

For an alternative spectral approach, I adopted the Chebyshev- τ method (Lanczos, 1956; Gottlieb and Orszag, 1977). The Chebyshev- τ velocity continuation algorithm consists of the following steps:

1. Transform the regular grid in t to Gauss-Lobato collocation points, required for the fast Chebyshev transform. First, a new variable ξ is introduced by the shift transform:

$$\xi = 1 - \frac{2t^2}{T^2} \quad (10)$$

so that the domain $0 \leq t \leq T$ is mapped into the domain $1 \geq \xi \geq -1$. Second, the ξ grid points are distributed regularly in the cosine projection: $\xi_j = \cos(\frac{\pi j}{N})$, $j = 0, 1, 2, \dots, N$.

2. Transform the initial image $P_0(x, t)$ into the Chebyshev space in ξ and Fourier transform in x , using the FFT algorithm. The Chebyshev-Fourier representation of $P_0(x, t)$ is

$$P_0(x, t) = \sum_{k=-N_x/2}^{N_x/2-1} \sum_{j=0}^{N_t} \hat{P}_{kj} T_j(\xi) e^{ikx}, \quad (11)$$

where T_j denotes the Chebyshev polynomial of degree j .

3. Apply equation (1) to advance the image in velocity v . It is convenient to rewrite this equation in the form

$$\frac{\partial P}{\partial v} = \frac{vT^2}{4} \int d\xi \frac{\partial^2 P}{\partial x^2}. \quad (12)$$

In the Chebyshev- τ domain, the double differentiation in x is performed by multiplying the Fourier transform of P by $-k^2$, and integration in ξ is performed as a direct operations on the Chebyshev coefficients. In particular, if $\sum_{j=0}^N a_j T_j(\xi)$ is the Chebyshev representation of the function $f(\xi)$, then the coefficients b_j of $\int f(\xi) d\xi$ are defined by the relation

$$2j b_j = c_{j-1} a_{j-1} - a_{j+1} \quad (13)$$

where $c_0 = 2$, $c_j = 0$ for $j < 0$, and $c_j = 1$ for $j > 0$. The constant of integration (and, correspondingly, the coefficient b_0) can be found at each velocity step from the boundary conditions (2), which are transformed to the form

$$P|_{\xi=-1} = \sum_{j=0}^{N_t} \hat{P}_{kj} (-1)^j = 0. \quad (14)$$

For the velocity advancement I used an implicit Crank-Nicolson scheme, which is unconditionally stable independent of the velocity step size. By writing equation (12) in the matrix form

$$\frac{\partial \mathbf{P}}{\partial v} = \mathbf{A} \mathbf{P}, \quad (15)$$

the Crank-Nicolson advancement is represented by the equation

$$\mathbf{P}_{v+dv} = \left(\mathbf{I} - \mathbf{A} \frac{dv}{2} \right)^{-1} \left(\mathbf{I} + \mathbf{A} \frac{dv}{2} \right) \mathbf{P}_v, \quad (16)$$

where \mathbf{I} is the identity matrix. The inverted matrix $\left(\mathbf{I} - \mathbf{A} \frac{dv}{2} \right)$ has a tridiagonal structure, except for the first row, implied by the boundary condition (14). A careful treatment of the boundary condition by the matrix-bordering method (Faddeev and Faddeeva, 1963; Boyd, 1989) allows for an efficient inversion at a tridiagonal solver speed.

4. Transform the result of the velocity advancement back to the physical domain.
5. Transform the grid back to being regularly space in t .

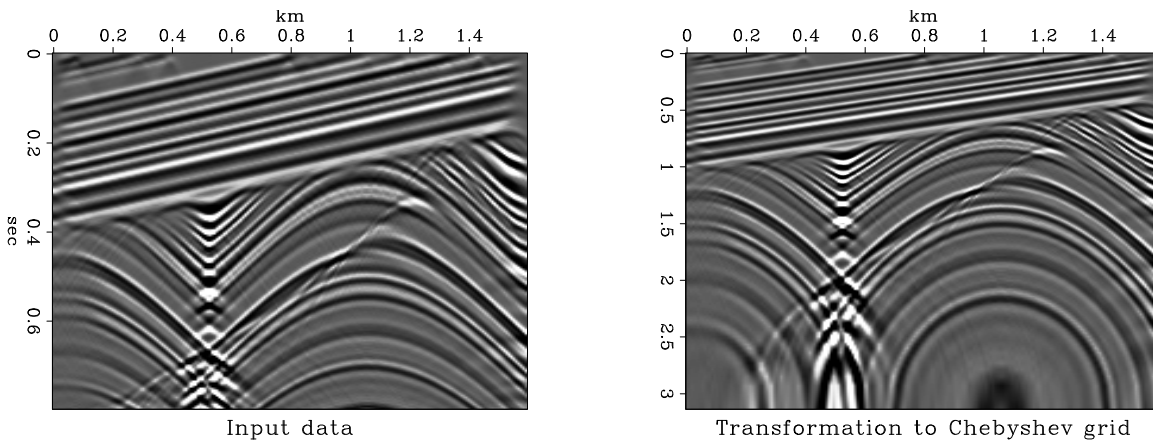


Figure 6: Synthetic seismic data before (left) and after (right) transformation to the Chebyshev grid in squared time. `velspec-cheb1` [ER]

The first advantage of the Chebyshev approach comes from the better conditioning of the grid transform. Figure 6 shows the synthetic data before and after the grid transform. Figure 7 shows a reconstruction of the original data after transforming back from the Chebyshev grid (Gauss-Lobato collocation points). The difference with the original image is negligibly small.

The second advantage is the compactness of the Chebyshev representation. Figure 8 shows the data after the decomposition into Chebyshev polynomials in ξ and Fourier transform in x . We observe a very rapid convergence of the Chebyshev representation: a relatively small number of polynomials suffices to represent the data.

The third advantage is the proper handling of the non-periodic boundary conditions. Figure 9 shows the velocity continuation impulse responses, computed by the Chebyshev method. As expected, no wraparound artifacts occur on the time axis, and the accuracy of the result is noticeably higher than in the case of finite differences (Figure 1).

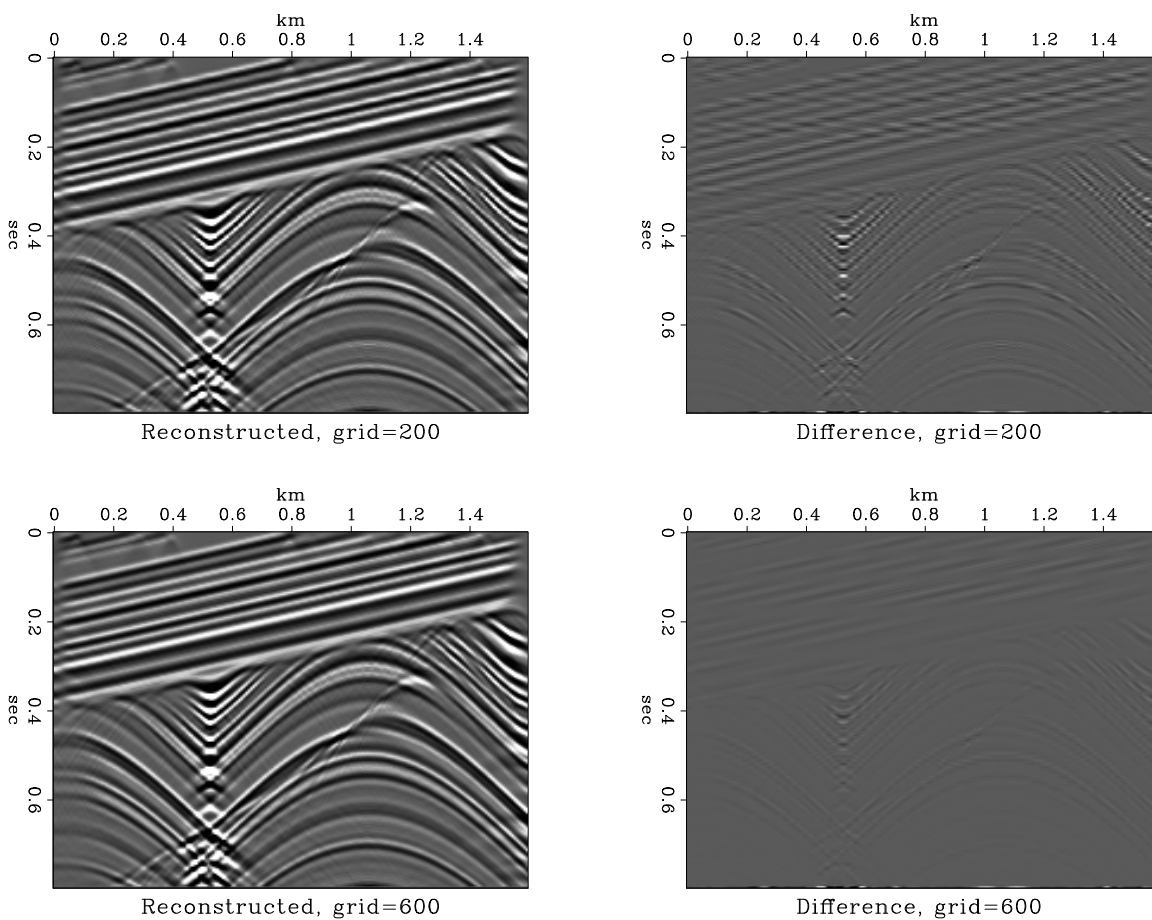


Figure 7: The left plots show the reconstruction of the original data after transforming back from the Chebyshev grid to the original t grid. The right plots show the difference with the original model. Top: using the original grid size ($N_t = 200$). Bottom: increasing the grid size by a factor of three. `velspec-cheb1-inv` [ER]

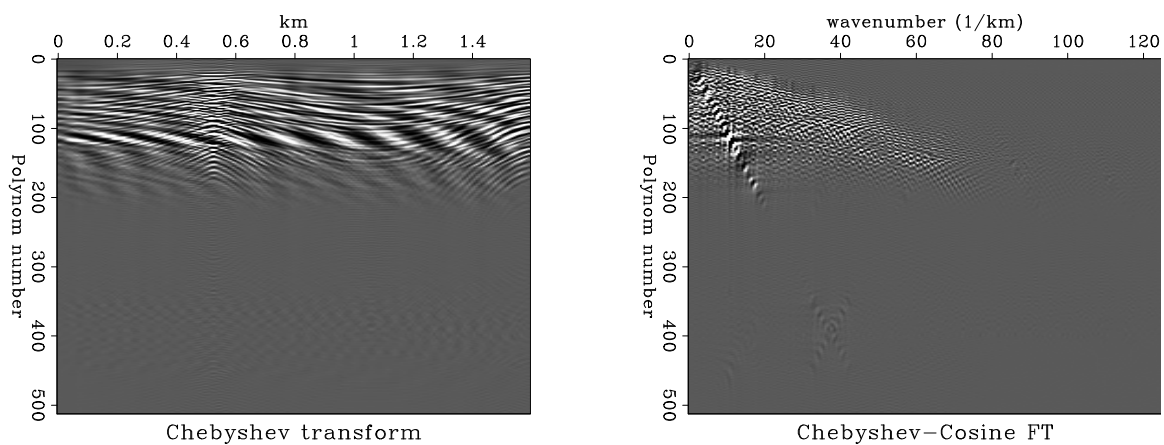


Figure 8: Left: Synthetic data after Chebyshev transform. Right: the real part of the Fourier transform in the space coordinate. `velspec-cheb1-fft` [ER]

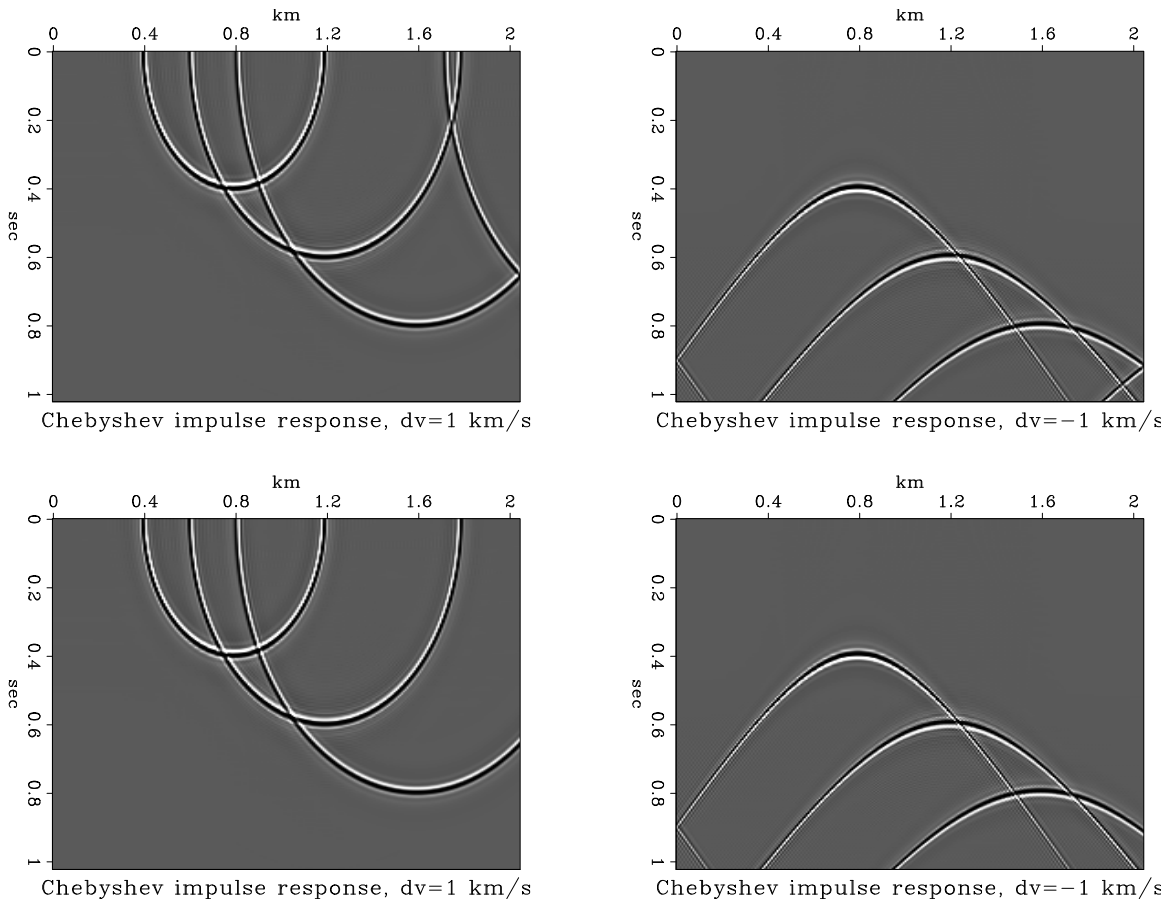


Figure 9: Impulse responses (Green's functions) of velocity continuation, computed by the Chebyshev- τ method. Top: without zero padding, bottom: with zero padding on the x axis. The left plots correspond to continuation to a larger velocity (+1 km/sec); the right plots, smaller velocity, (-1 km/sec). `velspec-cheb-impl` [ER]

CONCLUSIONS

I have applied two spectral methods for a numerical solution of the velocity continuation problem.

The Fourier method is attractive because of its numerical efficiency. However, it requires additional computational effort to suppress numerical artifacts: the inaccuracy of the grid transform and the artificial periodicity in the physical space.

The Chebyshev- τ method is free of most of these difficulties, although its overall efficiency can be slightly inferior to that of the Fourier method.

Both methods possess a “spectral” accuracy, which is highly desired if accuracy is a concern.

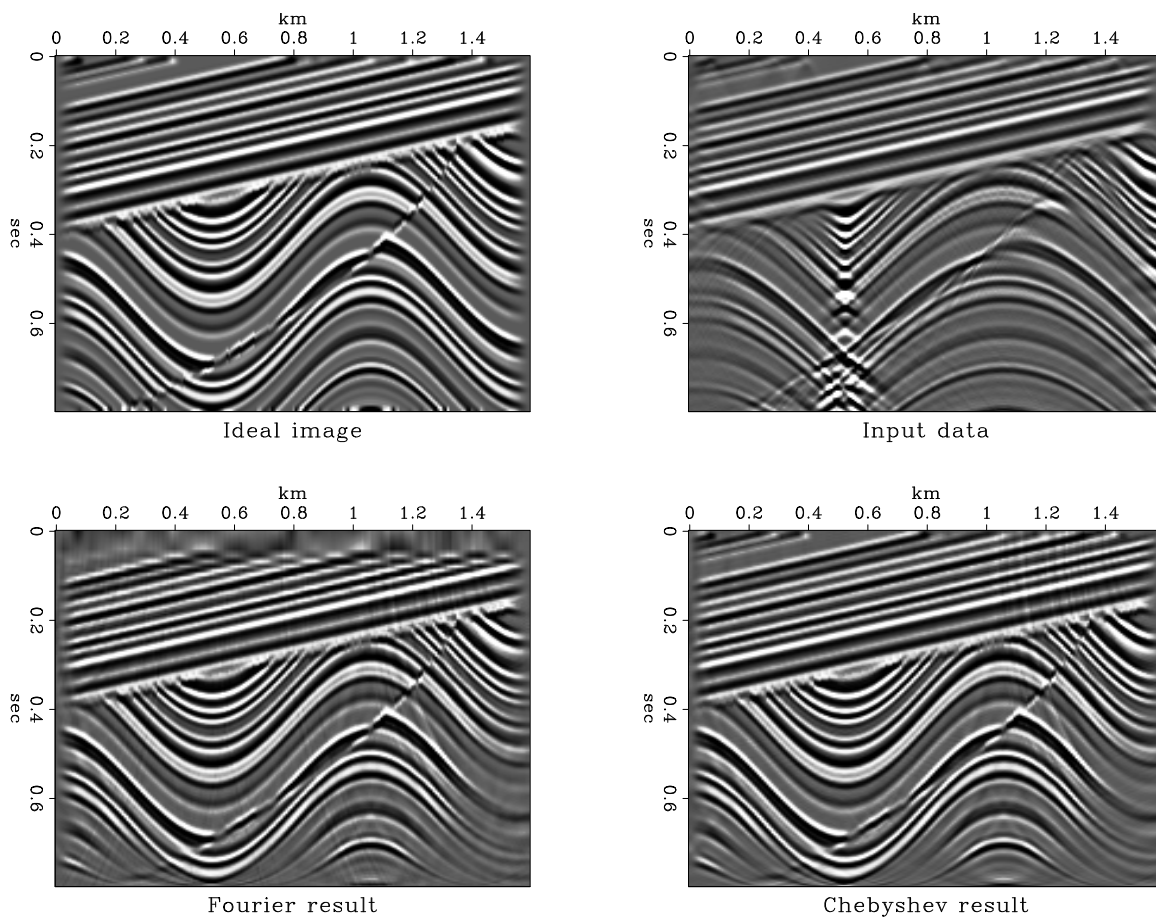


Figure 10: Top left: synthetic model (the ideal image). Top right: synthetic data. Bottom left: the result of velocity continuation with the Fourier method. Bottom right: the result of velocity continuation with the Chebyshev method. `velspec-mig-impl` [ER]

Figure 10 compares the results of velocity continuation with different methods. The top left plot shows an implied subsurface model (an “ideal image”). The top right plot is the corresponding synthetic data. The bottom left plot is the output of the Fourier method, and

the bottom right plot is the output of the Chebyshev method. The Fourier result shows a poor quality in the shallow part (caused by subsampling in the t^2 grid). The wraparound artifacts were suppressed by a zero-padding correction. The quality of the Chebyshev result is noticeably higher. It is close to the best possible accuracy, under the natural limitations of seismic resolution.

REFERENCES

- Boyd, J. P., 1989, Chebyshev and Fourier spectral methods: Springer-Verlag.
- Claerbout, J. F., 1986a, Pseudo unitary NMO tutorial: SEP-48, 347–350.
- Claerbout, J. F., 1986b, Velocity extrapolation by cascaded 15 degree migration: SEP-48, 79–84.
- Claerbout, J. F., 1995, Basic Earth Imaging: Stanford Exploration Project.
- Claerbout, J., 1997, Multidimensional recursive filters via a helix: SEP-95, 1–13.
- Courant, R., 1962, Methods of mathematical physics: Interscience Publishers, New York.
- Etgen, J., 1990, Residual prestack migration and interval velocity estimation: Ph.D. thesis, Stanford University.
- Faddeev, D. K., and Faddeeva, V. N., 1963, Computational methods of linear algebra: Dover.
- Fomel, S., and Claerbout, J. F., 1997, Exploring three-dimensional implicit wavefield extrapolation with the helix transform: SEP-95, 43–60.
- Fomel, S. B., 1994, Method of velocity continuation in the problem of temporal seismic migration: Russian Geology and Geophysics, 35, no. 5, 100–111.
- Fomel, S., 1996, Migration and velocity analysis by velocity continuation: SEP-92, 159–188.
- Fomel, S., 1997, Velocity continuation and the anatomy of residual prestack migration: 67th Ann. Internat. Meeting, Soc. Expl. Geophys., Expanded Abstracts, 1762–1765.
- Gottlieb, D., and Orszag, S. A., 1977, Numerical analysis of spectral methods: Theory and applications: SIAM.
- Hubral, P., Tygel, M., and Schleicher, J., 1996, Seismic image waves: Geophysical Journal International, 125, 431–442.
- Lanczos, C., 1956, Applied analysis: Prentice-Hall.
- Larner, K., and Beasley, C., 1987, Cascaded migrations—Improving the accuracy of finite-difference migration: Geophysics, 52, no. 5, 618–643.
- Li, Z., 1986, Cascaded one step fifteen degree migration versus Stolt migration: SEP-48, 85–100.

- Rothman, D. H., Levin, S. A., and Rocca, F., 1985, Residual migration – applications and limitations: *Geophysics*, **50**, no. 1, 110–126.
- Schleicher, J., Hubral, P., Hoecht, G., and Liptow, F., 1997, Seismic constant-velocity remigration: *Geophysics*, **62**, 589–597.
- Schneider, W. A., 1978, Integral formulation for migration in two-dimensions and three-dimensions: *Geophysics*, **43**, no. 1, 49–76.
- Stolt, R. H., 1985, Migration by Fourier transform: *Geophysics*, **50**, no. 11, 2219–2244.